

# ELMAG: A Monte Carlo simulation of electromagnetic cascades on the extragalactic background light and in magnetic fields

M. Kachelrieß<sup>a</sup>, S. Ostapchenko<sup>a,b</sup>, and R. Tomàs<sup>c</sup>

<sup>a</sup>*Institutt for fysikk, NTNU, Trondheim, Norway*

<sup>b</sup>*D. V. Skobeltsyn Institute of Nuclear Physics, Moscow State University, Russia*

<sup>c</sup>*II. Institut für Theoretische Physik, Universität Hamburg, Germany*

---

## Abstract

A Monte Carlo program for the simulation of electromagnetic cascades initiated by high-energy photons and electrons interacting with extragalactic background light (EBL) is presented. Pair production and inverse Compton scattering on EBL photons as well as synchrotron losses and deflections of the charged component in extragalactic magnetic fields (EGMF) are included in the simulation. Weighted sampling of the cascade development is applied to reduce the number of secondary particles and to speed up computations. As final result, the simulation procedure provides the energy, the observation angle, and the time delay of secondary cascade particles at the present epoch. Possible applications are the study of TeV blazars and the influence of the EGMF on their spectra or the calculation of the contribution from ultrahigh energy cosmic rays or dark matter to the diffuse extragalactic gamma-ray background. As an illustration, we present results for deflections and time-delays relevant for the derivation of limits on the EGMF.

**Keywords:** Electromagnetic cascades, extragalactic background light, extragalactic magnetic fields.

---

## PROGRAM SUMMARY

*Manuscript Title:* ELMAG: A Monte Carlo simulation of electromagnetic cascades on the extragalactic background light and in magnetic fields

*Program Title:* ELMAG 1.01

*Journal Reference:*

*Catalogue identifier:*

*Licensing provisions:*

*Programming language:* Fortran 95

*Computer:* Any computer with Fortran 95 compiler

*Operating system:* Any system with Fortran 95 compiler

*RAM:* 4 Mbytes

*Number of processors used:* arbitrary using the MPI version

*Supplementary material:* see <http://elmag.sourceforge.net/>

*Keywords:* Electromagnetic cascades, extragalactic background light, extragalactic magnetic fields

*Classification:* 11.3 Cascade and Shower Simulation, 11.4 Quantum Electrodynamics

*Nature of problem:* Calculation of secondaries produced by electromagnetic cascades on the extragalactic background light (EBL)

*Solution method:* Monte Carlo simulation of pair production and inverse Compton scattering on EBL photons; two parametrisations from Ref. [1] can be chosen as EBL; weighted sampling of the cascading secondaries; recording of energy, observation angle and time delay of secondary particles at the present epoch.

*Restrictions:* Deflections and time-delays are calculated in the small-angle approximation.

*Unusual features:*

*Additional comments:*

*Running time:* 400 seconds for  $10^3$  photons injected at redshift  $z = 0.2$  with energy  $E = 100$  TeV using one Intel(R) Core(TM) i7 CPU with 2.8 GHz.

## References

- [1] T. M. Kneiske and H. Dole, *Astron. Astrophys.* **515** (2010) A19 [arXiv:1001.2132 [astro-ph.CO]].

## 1. Introduction

The Universe is opaque to the propagation of  $\gamma$ -rays with energies in the TeV region and above [1]. Such photons are absorbed by pair production on the extragalactic background light (EBL) [2–5], consisting mainly of infrared light and the cosmic microwave background (CMB). As a result the photon flux at energies  $E \gtrsim 10$  TeV from distant sources as e.g. blazars is significantly attenuated on the way from the source to the Earth. High-energy photons are however not really absorbed but initiate electromagnetic cascades in the intergalactic space, via the two processes

$$\gamma + \gamma_b \rightarrow e^+ + e^- \quad (1)$$

$$e^\pm + \gamma_b \rightarrow e^\pm + \gamma. \quad (2)$$

The cascade develops very fast until it reaches the pair creation threshold at  $s_{\min} = 4E_\gamma \varepsilon_\gamma = 4m_e^2$  with  $\varepsilon_\gamma$  as the characteristic energy of the background photons  $\gamma_b$ . Electrons<sup>2</sup> continue to scatter on EBL photons in the Thomson regime with an interaction length of a few kpc, producing photons with average energy

$$E_\gamma = \frac{4}{3} \frac{\varepsilon_\gamma E_e^2}{m_e^2} \approx 3 \text{ GeV} \left( \frac{E_e}{1 \text{ TeV}} \right)^2 \quad (3)$$

using  $\varepsilon_\gamma = 2.7 T_{\text{CMB}} \approx 6.3 \times 10^{-4} \text{ eV}$  as the typical energy of CMB photons.

The resulting shape of the energy spectrum of the diffuse photon flux  $J_\gamma$  can be estimated analytically [6] for a monochromatic background as

$$J_\gamma(E_\gamma) = \begin{cases} K(E_\gamma/E_x)^{-3/2} & \text{for } E_\gamma \leq E_x, \\ K(E_\gamma/E_x)^{-2} & \text{for } E_x \leq E_\gamma \leq E_{\min}, \\ 0 & \text{for } E_\gamma > E_{\min}. \end{cases}$$

Here,  $E_{\min} = m_e^2/\varepsilon_\gamma$  is the threshold energy for pair-production, while  $E_\gamma \leq E_x$  is the energy region where the number of electrons remains constant. Since the last generation of  $e^+e^-$  pairs produced share the initial energy equally,  $E_e = E_{\min}/2$ , this transition energy is given by  $E_x = 4\varepsilon_\gamma E_e^2/(3m_e^2) = E_{\min}/3$ . Thus for a monochromatic background the plateau region characterised by an  $1/E_\gamma^2$  spectrum extends only over one third of an energy decade.

A better analytical description of the cascade development in the EBL uses a dichromatic photon gas, with  $\varepsilon_{\text{CMB}} = 6.3 \times 10^{-4} \text{ eV}$  and  $\varepsilon_{\text{IR}} = 1 \text{ eV}$  as typical energies for the CMB and the (second) peak of the IR background, respectively. Below one half of the threshold energy of pair production on the IR,  $E_e \approx E_{\min, \text{IR}}/2 = m_e^2/(2\varepsilon_{\text{IR}}) \approx 1.3 \times 10^{11} \text{ eV}$ , the number of electrons remains constant. In the intermediate regime,  $E_{\min, \text{IR}} \lesssim E \lesssim E_{\min, \text{CMB}}$ , electrons are Compton scattering on CMB photons in the Thomson regime, while photons are still producing  $e^+e^-$  pairs on IR photons. Thus the energy  $E_x$  below which no additional electrons are injected in the cascade is given by

$$E_x = \frac{4}{3} \frac{\varepsilon_{\text{CMB}} E_e^2}{m_e^2} = \frac{1}{3} \frac{\varepsilon_{\text{CMB}}}{\varepsilon_{\text{IR}}} E_{\min, \text{IR}} \approx 50 \text{ MeV}. \quad (4)$$

Let us now compare how well this qualitative picture agrees with the cascade spectrum calculated with our Monte Carlo simulation. Figure 1 shows the results obtained with ELMAG for the diffuse spectrum of secondary photons produced by photons injected with energy  $E = 10^{14} \text{ eV}$  at redshift  $z = 0.02$  and  $z = 0.15$ . We note first that the slope of the photon spectrum below  $E_x$  and the obtained value of  $E_x$  agree very well for both distances with the prediction in the simple “dichromatic model,” although the latter assumes an infinite number of interactions. In contrast, both the extension and the shape of the plateau region are less universal: The smaller the distance to the source, the less pronounced occurs the steepening of the photon spectrum from the  $E^{-1.5}$  Thomson slope towards the predicted  $1/E^2$

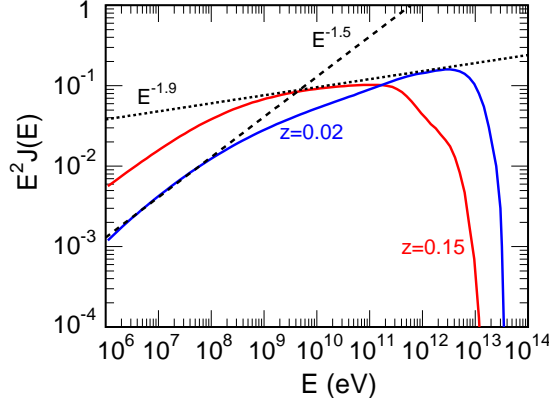


Figure 1: The (normalised) diffuse photon flux  $E^2 J(E)$  for two sources injecting photons with energy  $E = 10^{14}$  eV at redshift  $z = 0.02$  (—) and  $z = 0.15$  (—), respectively.

plateau. However, the deviation of the slope from the prediction,  $E^{-1.9}$  versus  $E^{-2}$ , is minor already for distances of  $\sim 500$  Mpc.

An important application of electromagnetic cascades is the calculation of various contributions to the extragalactic diffuse gamma-ray background (EGRB). Since the Universe acts as a calorimeter for electromagnetic radiation, accumulating it in the MeV–TeV range, the measured EGRB limits all processes during the history of the Universe that inject electromagnetic energy above the pair creation threshold. Examples for such processes are photo-pion and  $p + \gamma_{\text{CMB}} \rightarrow p + e^+ + e^-$  pair-production of UHECR protons interacting with the cosmic microwave background (CMB) [7], the decay or annihilation of (superheavy) dark matter or of topological defects [8]. Another important application of electromagnetic cascades is the calculation of spectra from point sources as TeV blazars. If the spectra of such sources extend to sufficiently high energies, emitted photons interact with the EBL. The charged component of these cascades is deflected by extragalactic magnetic fields (EGMF), leading potentially to halos around point sources [9–12], to delayed echos of flaring emission [13] and influences the observed energy spectrum [14]. A detailed modelling of the electromagnetic cascade process is thus not only necessary to connect the observed energy spectra of TeV sources with their intrinsic spectra, but provides also information about EGMFs.

The extremely small interaction length compared to typical source distances from hundreds of Mpc to Gpc means that a large number  $n$  of interaction steps has to be simulated using a Monte Carlo approach. The exponential growth of the number  $N = 2^n$  of secondaries aggravates the computational load in a brute-force Monte Carlo approach. The Monte Carlo program presented here uses weighted sampling of the cascade development to reduce efficiently the number of secondary particles which are traced explicitly. For maximally weighted sampling, the number of secondaries stays on average constant as function of interaction steps. Synchrotron losses and deflections of the charged component in extragalactic magnetic fields (EGMF) are included in the simulation too. The version presented here is restricted to the limit of small deflections.

## 2. Modelling of the cascade process

### 2.1. Interaction rate of photons and electrons

The interaction rate  $R_\gamma(E, z)$  of photons with energy  $E$  at redshift  $z$  can be connected to the pair-production cross section  $\sigma_{\text{pair}}(s)$  and the spectral density of background photons  $n_\gamma(E, z)$  as

$$R_\gamma(E, z) = \frac{1}{2} \int_0^\infty dE' n_\gamma(E', z) \int_{-1}^1 d\mu (1 - \mu) \sigma_{\text{pair}}(s) \Theta(s - s_{\text{min}})$$

<sup>1</sup>We use natural units,  $\hbar = c = k_B = 1$ , throughout the text.

<sup>2</sup>We call from now on electrons and positrons collectively electrons.

$$= \frac{1}{8E^2} \int_{s_{\min}}^{s_{\max}(E)} ds \, s \, \sigma_{\text{pair}}(s) I_{\gamma}\left(\frac{s}{4E}, z\right), \quad (5)$$

where we introduced the auxiliary function

$$I_{\gamma}(E_{\min}, z) = \int_{E_{\min}}^{E_{\max}} \frac{dE'}{E'^2} n_{\gamma}(E', z). \quad (6)$$

Here we have also assumed that the EBL, as any truly diffuse background, is isotropic.

The c.m. energy squared in a  $\gamma\gamma$  interaction is  $s = 2EE'(1 - \mu)$  with  $\mu = \cos \vartheta$ , while the integration limits are given by the pair production threshold  $s_{\min} = 4m_e^2$  and  $s_{\max}(E) = 4EE_{\max}$  with  $E_{\max} \sim 14 \text{ eV}$  as the high energy cutoff of the EBL background. The well-known pair-production cross section  $\sigma_{\text{pair}}(s)$  is given by

$$\sigma_{\text{pair}}(s) = \frac{3}{4} \sigma_{\text{Th}} \frac{m_e^2}{s} \left[ (3 - \beta^4) \ln \frac{1 + \beta}{1 - \beta} - 2\beta(2 - \beta^2) \right], \quad (7)$$

with  $\sigma_{\text{Th}} = 8\pi\alpha^2/(3m_e^2)$  as Thomson cross section and  $\beta = \sqrt{1 - 4m_e^2/s}$ .

Electrons emit in the Thomson regime mainly soft photons, cf. Eq. (3). To speed up the simulation, we include therefore as discrete interactions only those which produce secondary photons above an arbitrary energy threshold  $E_{\text{thr}}$ . The remaining soft interactions are integrated out and included as continuous energy loss. Thus we define the interaction rate  $R_e(E, z)$  of an electron with energy  $E$  at redshift  $z$  as

$$\begin{aligned} R_e(E, z) &= \frac{1}{2} \int_0^{\infty} dE' n_{\gamma}(E', z) \int_{-1}^1 d\mu (1 - \beta\mu) \sigma_{\text{C}}(s, \varepsilon) \Theta(s - s_{\min}(\varepsilon)) \\ &= \frac{1}{8\beta E^2} \int_{s_{\min}(\varepsilon)}^{s_{\max}(E)} ds (s - m_e^2) \sigma_{\text{C}}(s, \varepsilon) I_{\gamma}\left(\frac{s - m_e^2}{2E(1 + \beta)}, z\right) \end{aligned} \quad (8)$$

with  $\varepsilon = E_{\text{thr}}/E$ ,  $\beta = \sqrt{1 - m_e^2/E^2}$ , and  $s = m_e^2 + 2EE'(1 - \beta\mu)$ . The integration limits are given by  $s_{\min}(\varepsilon) = m_e^2/(1 - \varepsilon)$  and  $s_{\max}(E) = m_e^2 + 2EE_{\max}(1 + \beta)$ , while the Compton scattering cross section  $\sigma_{\text{C}}(s, \varepsilon)$  integrated above the threshold  $\varepsilon$  is given by

$$\begin{aligned} \sigma_{\text{C}}(s, \varepsilon) &= \frac{3}{4} \sigma_{\text{Th}} y_{\min} \frac{y_{\max} - y_{\min}}{1 - y_{\min}} \left[ \frac{\ln(y_{\max}/y_{\min})}{y_{\max} - y_{\min}} \left( 1 - \frac{4y_{\min}(1 + y_{\min})}{(1 - y_{\min})^2} \right) \right. \\ &\quad \left. + \frac{4(y_{\min}/y_{\max} + y_{\min})}{(1 - y_{\min})^2} + \frac{y_{\max} + y_{\min}}{2} \right]. \end{aligned} \quad (9)$$

Here,  $y_{\min} = m_e^2/s$  and  $y_{\max} = 1 - \varepsilon$  are respectively the minimal and the maximal energy fractions of the secondary electron.

In turn, for the electron energy loss per unit distance due to the emission of photons of energies  $E < E_{\text{thr}}$  one obtains

$$\begin{aligned} \frac{dE_{\text{ICS/thr}}}{dx}(s, \varepsilon) &= \frac{3}{4} \sigma_{\text{Th}} y_{\min} \frac{1 - y_{\max}}{1 - y_{\min}} \left[ \left( \frac{\ln(1/y_{\max})}{1 - y_{\max}} - 1 \right) \left( 1 - \frac{4y_{\min}(1 + 2y_{\min})}{(1 - y_{\min})^2} \right) \right. \\ &\quad \left. + \frac{1}{6}(1 - y_{\max})(1 + 2y_{\max}) + \frac{2y_{\min}(1 + 2y_{\min}/y_{\max})(1 - y_{\max})}{(1 - y_{\min})^2} \right]. \end{aligned} \quad (10)$$

In the left panel of Fig. 2 we show the interaction rates  $R_i$  of electrons and photons at the present epoch as function of energy. The difference between the “best-fit” and the “lower-limit” EBL from Ref. [5] becomes visible in the interaction rate  $R_{\gamma}$  of photons only in the energy range below  $10^{14} \text{ eV}$ . The interaction rate  $R_e$  of electrons is shown only for the “best-fit” EBL but for two different values of the threshold  $E_{\text{thr}}$  used in the Compton scattering cross section,  $E_{\text{thr}} = 3 \times 10^4 \text{ eV}$  and  $E_{\text{thr}} = 3 \times 10^6 \text{ eV}$ . Note that while  $E_{\text{thr}} = 3 \times 10^6 \text{ eV}$  leads already below  $10^{11} \text{ eV}$  to strong deviations from the Thomson scattering cross section, the resulting photon spectrum is influenced by the threshold mainly at energies in the MeV range and below, cf. Eq. (3).

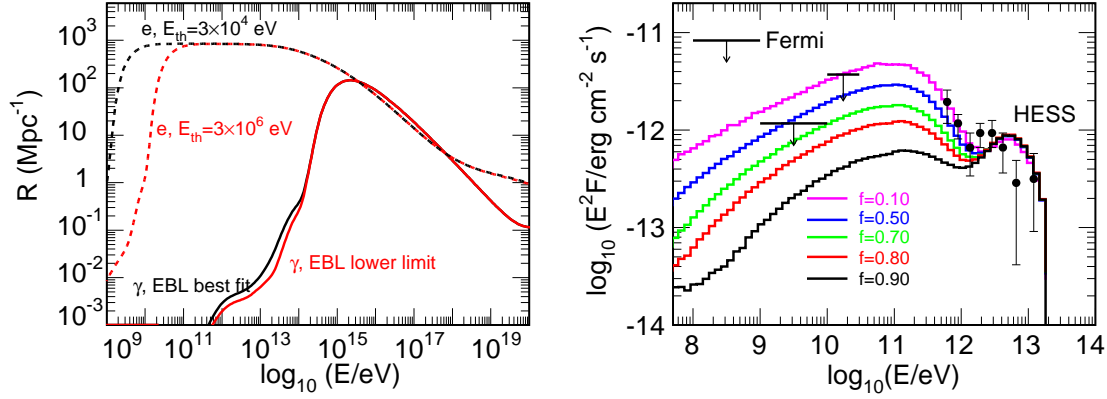


Figure 2: Left: Interaction rate  $R$  at  $z = 0$  as function of the energy  $E$  for electrons with  $E_{\text{th}} = 3 \times 10^4 \text{ eV}$  and  $E_{\text{th}} = 3 \times 10^6 \text{ eV}$  and for photons with the “best-fit” and the “lower-limit” EBL from Ref. [5]. Right: Fluence contained inside the 95% confidence contour of the PSF of Fermi-LAT as function of energy for EGMF with top-hat profile and filling factor  $f$  varying from  $f = 0.1$  to  $f = 0.9$  with  $E_{\text{max}} = 20 \text{ TeV}$ .

## 2.2. Interactions

The modelling of  $\gamma\gamma$  and  $e\gamma$  interactions starts from sampling the c.m. energy squared  $s$  of the collision according to the integrands of Eqs. (5) and (8), respectively. Technically, the rejection method is used as in most other cases to choose  $s$  according to its probability distribution: The value of  $s$  is first sampled logarithmically in the interval  $[s_{\text{min}}, s_{\text{max}}]$ , then the choice is accepted with the probability proportional to  $s$  times the integrand of Eq. (5) and (8), or otherwise rejected.

For given  $s$ , the energy fraction  $y$  of the lowest energy secondary lepton (electron or positron) in the pair production process is sampled according to the corresponding differential cross section

$$\frac{d\sigma_{\text{pair}}(s, y)}{dy} \propto \frac{1}{y} \left[ \frac{y^2}{1-y} + 1 - y + \frac{1-\beta^2}{1-y} - \frac{(1-\beta^2)^2}{4y(1-y)^2} \right] / [1 + 2\beta^2(1-\beta^2)], \quad (11)$$

with  $\beta = \sqrt{1 - 4m_e^2/s}$ . The other secondary lepton has then the energy fraction  $1 - y$ . Similarly, the energy fraction  $y$  of the secondary electron in the inverse Compton process is sampled according to the differential cross section

$$\frac{d\sigma_{\text{ICS}}(s, y)}{dy} \propto \frac{1}{y} \left[ \frac{1+y^2}{2} - \frac{2y_{\text{min}}(y-y_{\text{min}})(1-y)}{y(1-y_{\text{min}})^2} \right], \quad (12)$$

with  $y_{\text{min}} = m_e^2/s$ .

## 2.3. Stacking and weighted sampling

The produced secondary particles are then subject to a weighted sampling procedure: A secondary particle carrying the fraction  $y$  of the parent energy is discarded with the probability  $(1 - y^{\alpha_{\text{sample}}})$ , or added with the probability  $y^{\alpha_{\text{sample}}}$  to the stack. Depending on the choice of the sampling parameter ( $0 \leq \alpha_{\text{sample}} \leq 1$ ) either all the secondaries are kept in the cascade ( $\alpha_{\text{sample}} = 0$ ) or only some representative ones are retained. In particular, one secondary per interaction is retained on average for the default value  $\alpha_{\text{sample}} = 1$ . As compensation, each particle in the cascade acquires a weight  $w$  which is augmented after each interaction as  $w \rightarrow w/y^{\alpha_{\text{sample}}}$ . The particles in the stack are ordered according to their energies. After the interaction, the lowest energy particle is extracted from the stack and traced further in the cascade process.

The optimal value of  $\alpha_{\text{sample}}$  depends on the typical energy of the injected photons. If the latter is so low that the cascades consists on average of only few steps, reducing  $\alpha_{\text{sample}}$  may be advantageous because the fluctuations are thereby reduced.

#### 2.4. Synchrotron losses

Synchrotron energy losses of electrons are accounted for in the continuous energy loss approximation using the interpolation formula [23],

$$\frac{dE}{dx} \approx \frac{m_e^2 \chi^2}{[1 + 4.8(1 + \chi) \ln(1 + 1.7\chi) + 3.44\chi^2]^{2/3}}, \quad (13)$$

with  $\chi = (p_\perp/m_e)(B/B_{\text{cr}})$ , where  $p_\perp$  denotes the momentum perpendicular to the magnetic field and  $B_{\text{cr}} = 4.14 \times 10^{13}$  G the critical magnetic field.

#### 2.5. Angular deflection and time delay

For the energies considered,  $E_\gamma \gtrsim \text{MeV}$  and  $E_e \gtrsim 10 \text{ GeV}$ , secondary particles are emitted in the forward direction. Thus the angular deflection of the cascade particles results from the deflections of electrons in the extragalactic magnetic field (EGMF). If the coherence scale of the EGMF is much larger than electron mean free path  $\lambda_e = R_e^{-1}$ , an elementary deflection angle of  $i$ -th electron in the cascade chain can be calculated assuming the field to be regular over the distance  $d_i$  travelled by the electron,

$$\beta_i \simeq 0.52^\circ \left( \frac{p_\perp}{\text{TeV}} \right)^{-1} \left( \frac{d_i}{10 \text{ kpc}} \right) \left( \frac{B}{10^{-15} \text{ G}} \right), \quad (14)$$

with  $p_\perp$  being the momentum component perpendicular to the local direction of the magnetic field. Inside the patch  $j$  of a chosen coherence length, the deflection angles  $\beta_i$  per electron path are summed up coherently,  $\beta_j = \sum_i \beta_i$ . The deflections angles  $\beta_i$  per coherent magnetic field patch are then summed quadratically in the random-walk approximation to obtain as total deflection, i.e. the angle  $\beta$  between the initial and final photons in the cascade,

$$\beta = \sqrt{\sum_i \beta_i^2}, \quad (15)$$

In the small-angle approximation and assuming spherical symmetry, the angle  $\beta$  between the initial and final photons in the cascade is related to the emission angle  $\alpha$  and the observation angle  $\vartheta$  as  $\alpha = \beta - \vartheta$ , cf. Ref. [11].

As the energy of the cascade particles quickly degrades along the cascade chain, the largest contribution to  $\beta$  comes from the last electron in the chain. This allows us to approximate the corresponding geometry by a triangular configuration and to obtain as relation between  $\beta$  and  $\vartheta$

$$\sin \vartheta = \frac{x}{L} \sin \beta. \quad (16)$$

Here  $x$  refers to the distance from the source S to the point P where the final photon in the cascade branch has been created and  $L$  is the total distance between the source and the observer O. For small  $\vartheta$ , we thus have

$$\vartheta = \frac{x}{L} \sin \beta. \quad (17)$$

The time delay  $\Delta t_{\text{geo}}$  of photons with respect to the straight line propagation from the source is then

$$\Delta t_{\text{geo}} \simeq x(1 + \sin \alpha / \sin \vartheta) - L \simeq 2x(1 - x/L) \sin^2 \beta. \quad (18)$$

We add to this geometrical time delay  $\Delta t_{\text{geo}}$  the kinematical time delay  $\Delta t_{\text{kin}}$  due to velocity  $v < c$  of the electron, although the latter is usually negligible.

#### 2.6. Cosmology

The connection between redshift  $z$ , comoving distance  $r$  and light-travel time  $t$  calculated for a flat Friedmann-Robertson-Walker universe with  $\Omega_\Lambda = 0.7$  and  $\Omega_m = 0.3$  is contained in the file `redshift`.

### 3. Programme structure

The programme is distributed among the files `modules101.f90`, `user101.f90`, `init101.f90`, `elmag101.f90` and `aux101.f90`. The file `modules101.f90` contains the definition of internal variables, mathematical and physical constants; for standard applications of the programme no changes by the user are needed. The file `user101.f90` contains the input/output subroutines developed by the user for the desired task. An example file is discussed in Sec. 5. Data files of the used EBL backgrounds and the cosmological evolution of the universe are provided in the directory `Tables`. They are read by the subroutines `init_EBL(myid)`, `init_arrays(myid)` and the function `aintIR(E,z)` inside the file `init101.f90`. Then the function `w_EBL_density_tab(emin,zz)` tabulates the weighted background photon density  $I_\gamma$  defined in Eq. (6), followed by the tabulation of the interaction rate in the subroutine `rate_EBL_tab(e0,zz,icq)` and of the electron energy losses due to the emission of photons with energy below the threshold in `eloss_thr_tab(e0,zz,icq)`.

We discuss now in more detail the subroutines and functions of the file `elmag101.f90` which constitute the core of the programme:

- subroutine `cascade(icq,e00,weight0,z_in)`  
Follows the evolution of the cascade initiated by a photon ( $icq = 0$ ) or an electron/positron ( $icq = \pm 1$ ) injected at redshift  $z_{in}$  with energy  $e00$  and weight  $weight0$  until all secondary particles have energies below the energy threshold  $ethr$  or reached the observer at  $z = 0$ .
- subroutine `angle_delay(the2,xx,rcmb,theta,dt)`  
Determines the photon time-delay  $dt$  and the observation angle  $theta$  from the rms cascade deflection angle  $the2$  and the photon emission point  $xx$  by the parent electron/positron.
- subroutine `interaction(e0,x0,zz,t,weight,the1,the2,xxc,xx,dt,icq)`  
Handles one interaction with background photons: determines the c.m. energy  $sgam$  of the reaction via a call to `sample_photon` or `sample_electron(e0,zz,sgam,ierr)`, the energy fraction  $z$  of secondaries via a call to the functions `zpair(sgam)` or `zics(e0,sgam)`, and stores then the secondaries calling the subroutine `store_particle`.
- subroutine `store_particle(e0,x0,zz,t,ze,weight,the1,the2,xxc,xx,dt,icq)`  
Decides if a produced secondary is stored using weighted sampling; if yes, it adds the secondary to the array `event` and re-orders the array according to the particle energies.
- subroutine `get_particle(e0,x0,zz,t,weight,the1,the2,xxc,xx,dt,icq)`  
Reads the secondary with the lowest energy out of the array `event` and reduces the particle counter `jcmb` by one.
- subroutine `sample_photon(e0,zz,sgam,ierr)` and `sample_electron(e0,zz,sgam,ierr)`  
Determines the cms energy  $sgam$  of an interaction at redshift  $zz$ .
- double precision function `w_EBL_density(emin,zz)`  
Determines the weighted background photon density  $I_\gamma$  defined in Eq. (6).
- function `int_point(e0,x0,zz,icq)`  
Finds the next interaction point for interaction with EBL photons.
- function `sigpair(sgam)` and `sigics(e0,sgam)`  
Calculate the pair production and inverse Compton cross section, respectively.
- function `zpair(sgam)` and `zics(e0,sgam)`  
Determine the energy distribution in pair production and inverse Compton scattering, respectively.
- function `zsigics(e0,sgam)`  
Calculates the electron energy losses per unit distance due to photon emission below the chosen threshold in Compton scattering.

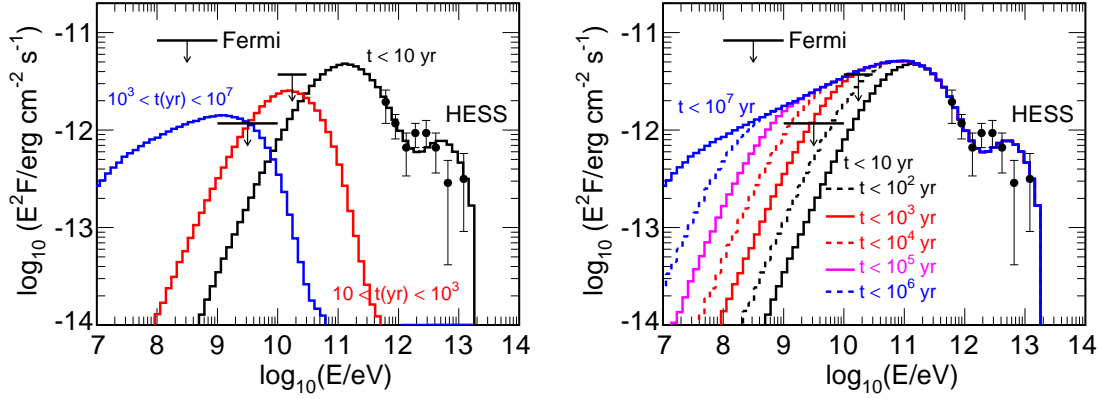


Figure 3: Fluence contained inside the 95% confidence contour of the PSF of Fermi-LAT as function of the time-delay for  $B = 10^{-17}$  G; left for individual time layers, right cumulative times.

- `function zloss(e0,zz)`  
Interpolates the integrated energy loss due to emission of photons below the threshold.
- `subroutine rate_EBL(e0,zz,icq)`  
Interpolates the interaction rates  $R_i$  on EBL photons.
- `function eloss_syn(E,begmf)`  
Calculates the synchrotron losses according to Eq. (13).
- `function themf(e0,dx,begmf)`  
Determines the deflection angle in the EGMF.

The file `aux101.f90` contains auxiliary functions, e.g. the random number generator `psran` from Ref. [24].

#### 4. Example input and output

The file `user101.f90` is an example file for the input/output subroutines which should be developed by the user for the desired task. We discuss now the example contained in the distribution.

##### 4.1. Example input

The input variables specified in the module `user_variables` are: the choice of the EBL model (`model`), the number of injected particles (`nmax`), the jet opening angle of the source in degrees (`th_jet`), the sampling parameter `a_smp`, the energy threshold `ethr` for Compton scattering, and the maximal photon energy `egmax`. The last two parameters serve also as minimal and maximal energy in the energy spectra produced as output. In subroutine `user_main(myid,nmax)` the initial redshift `z` and the particle type `icq` of the injected particles is fixed.

```

z = 0.14d0                                ! initial redshift
do nl=1,nmax
  call initial_particle(e0,weight)          ! generate initial energy
  icq = 0                                  ! (0 - gamma, +-1 - e+-)
  call cascade(icq,e0,weight,z)             ! starts e/m cascade
enddo

```

The subroutine `initial_particle(e0,weight)` chooses the energy and the weight of one initial particle in the energy range  $[e_{\min}, e_{\max}]$  according to a broken power-law with exponents `gam1` below `ebreak`, and `gam2` above.

The magnetic field  $B$  is modeled as patches of uniform field-strength  $|\mathbf{B}|$  of size  $l_{\text{coh}}$ . The value of the coherence length is fixed by the parameter `cohlnth` in module `user_variables`, the field-strength perpendicular to the propagation direction in the function `bemf(r)`.



#### 4.2. Example output

The energy `e0`, the observation angle `theta` and the time delay `dt` of secondary cascade particles with weight `weight` of type `icq` reaching the observer at  $z = 0$  are recorded by the subroutine `register(e0,theta,dt,weight,icq)` and binned in various data arrays defined in the module `user_result`. All data arrays exists in two versions, e.g. `spec(n_bin,0:1)` and `spec_tot(n_bin,0:1)`. Using MPI [15], the former arrays contain the result of a single process, which are summed by call `MPI_REDUCE` into `spec_tot(n_bin,0:1)`,

```
n_array = 2*n_bin
call MPI_REDUCE(spec,spec_tot,n_array,MPI_DOUBLE_PRECISION,MPI_SUM,0, & \
                MPI_COMM_WORLD,ierr)      ! sum individual arrays spec
```

Finally, the subroutine `user_output(n_max,n_proc)` writes the data arrays with the results in the files contained in the subdirectory `Data`.

The file `spec_diff` contains the normalised (diffuse) energy spectra of photons and electrons, in the format  $E/eV$ ,  $E^2 dN_\gamma/dE$  and  $E^2 dN_e/dE$ . The file `spec_95` includes the energy spectra of photons inside and outside the 95% area of the point-spread function of Fermi-LAT, in the format  $E/eV$ ,  $E^2 dN_\gamma/dE(\theta < \theta_{95})$  and  $E^2 dN_\gamma/dE(\theta > \theta_{95})$ . An approximation to the point-spread function of Fermi-LAT is defined in the function `thereg_en(en)`.

The right panel of Fig. 2 shows the energy spectra of photons arriving within the 95% area of the point-spread function of Fermi-LAT for different filling factors of the EGMF which can be chosen by the parameter `frac` in the function `bemf`. Otherwise the default values contained in the distributed file `user101.f90` are used. The photon fluence is compared to H.E.S.S. data [16] and upper limits from Fermi-LAT [17] for the TeV blazar 1ES 0229+200.

The files `spec_95.t` and `spec_95.c` contain the energy spectra of photons arriving within the 95% area of the point-spread function, with the time-delay binned in seven time intervals,  $t < 10$  yr,  $10 \text{ yr} < 10^2 \text{ yr}$ ,  $\dots t > 10^6 \text{ yr}$ . The file `spec_95.c` is the cumulative version of the distribution in `spec_95.t`. Figure 3 shows the fluence inside the 95% PSF of Fermi-LAT for an injection spectrum  $dN_\gamma/dE \propto E^{-2/3}$  at redshift  $z = 0.14$  with maximal energy  $E_{\text{max}} = 20 \text{ TeV}$ .

### 5. Possible extensions

We discuss four possible applications of the simulation ELMAG and the required extensions to perform them, ordered by the complexity of the necessary changes and additions.

*EGRB from dark matter decays or annihilations.* High-energy electrons and photons can be generated by decays or annihilations of sufficiently heavy dark matter particles. For instance, the annihilation mode  $XX \rightarrow e^+e^-$  of the dark matter particle  $X$  with mass  $m_X$  would correspond to the injection of two electrons with energy  $E_e = m_X$ . The only necessary addition for the calculation of the resulting EGRB is a subroutine choosing the injection point according to the so-called boost factor  $B(z)$  which accounts for the redshift dependent clustering of dark matter in galaxies. Additionally, the desired fragmentation functions  $dN_\gamma/dE$  of the  $X$  particles should be included into the subroutine `initial_particle` in the case of photons from hadronic decay or annihilation modes.

*EGRB from UHECRs and cosmogenic neutrinos.* The Greisen-Zatsepin-Kuzmin cutoff is a steepening of the proton spectrum at the energy  $E_{\text{GZK}} \approx (4 - 5) \times 10^{19} \text{ eV}$ , caused by photo-pion production on the CMB. An additional signature for the presence of extragalactic protons in the cosmic ray flux and their interaction with CMB photons is the existence of ultrahigh energy cosmogenic neutrinos produced by charged pion decays [18], while the corresponding flux of cosmogenic neutrinos from ultrahigh energy nuclei is suppressed. Photons and electrons from pion decay and  $p + \gamma_{\text{CMB}} \rightarrow p + e^+ + e^-$  pair-production lead to a contribution to the EGRB which can be used to limit cosmic rays (CR) models and fluxes of cosmogenic neutrinos. To perform this task, ELMAG has to be coupled to a program performing the propagation of ultrahigh energy cosmic rays which provides secondary electrons and photons from CR interactions as input. As the communication between the two program parts is restricted to calls of the subroutine `cascade(icq,e0,weight,z)`, such a combination should be straightforward. For an example where ELMAG was used in this context see Ref. [19].

*Extension to 3-dimensional cascades.* Going beyond the small-angle approximation requires to calculate the actual trajectory of electrons solving the Lorentz equation. Additionally, scalar quantities like `x`, `xxc`, `e0`, `begmf`, ... have to be changed into three-dimensional vectors and the type `one_event` in the module `stack` has to be adjusted. Finally, the image of a three-dimensional cascade can be calculated using the method described in Ref. [20]. For an illustration of possible applications of ELMAG to this problem see Ref. [21].

*Treatment of interactions in sources.* Photons and electrons are generated often in sources containing dense photon fields, as e.g. near the cores of active galactic nuclei. In this case, electromagnetic cascades take place on non-thermal, anisotropic photon backgrounds inside the source before the escaping particles cascade on the EBL. In order to describe both cascades on the EBL and inside the source, subroutines as e.g. `init_EBL` have to be doubled, adding a corresponding subroutine `init_source` for the photon field inside the source. All existing subroutines which depend on the chosen EBL (i.e. use `EBL_fit`) have to be adapted. In particular, the rejection mechanism in subroutines as e.g. `sample_photon` has to be adjusted. As a result, such an extension requires considerable work and thorough tests of the changed code. A short discussion of anisotropic photon fields is given in Ref. [22].

## 6. Summary

We presented a Monte Carlo program for the simulation of electromagnetic cascades initiated by high-energy photons and electrons interacting with the extragalactic background light. The program uses weighted sampling of the cascade development and treats Thomson scattering below a chosen threshold in the continuous energy loss approximation in order to speed up computations.

Possible applications are the study of TeV blazars and the influence of the EGMF on their spectra or the calculation of the contribution from ultrahigh energy cosmic rays or dark matter to the diffuse extragalactic gamma-ray background. As an illustration for possible applications we presented results for deflections and time-delays relevant for the derivation of limits on the EGMF studying the spectra of TeV blazars. Other possible applications include e.g. the calculation of the contribution from ultrahigh energy cosmic rays or dark matter annihilations to the diffuse extragalactic gamma-ray background.

## Acknowledgements

We are grateful to Venya Berezhinsky for valuable discussions and to Andrew Taylor for cross-checking some of our results. This work was partially supported by the program Romforskning of the Norwegian Research Council.

## References

- [1] R. J. Gould and G. P. Schreder, *Phys. Rev.* **155**, 1404 (1967); *ibid.*, 1408 (1967); F. W. Stecker, *Astrophys. Space Sci.* **6**, 377-389 (1970).
- [2] F. W. Stecker, M. A. Malkin and S. T. Scully, *Astrophys. J.* **648**, 774 (2006) [arXiv:astro-ph/0510449].
- [3] J. R. Primack, R. C. Gilmore and R. S. Somerville, *AIP Conf. Proc.* **1085**, 71 (2009) [arXiv:0811.3230 [astro-ph]].
- [4] A. Franceschini, G. Rodighiero and M. Vaccari, *Astron. Astrophys.* **487**, 837 (2008) [arXiv:0805.1841 [astro-ph]].
- [5] T. M. Kneiske and H. Dole, *Astron. Astrophys.* **515**, A19 (2010) [arXiv:1001.2132 [astro-ph.CO]].
- [6] V. S. Berezhinsky and A. Yu. Smirnov, *Astrophys. Sp. Sci.* **32**, 461 (1975); see also V. S. Berezhinsky *et al.*, *Astrophysics of Cosmic Rays* (Elsevier, Amsterdam (1990)) and V. S. Berezhinsky, *Nucl. Phys.* **B 380**, 478 (1992).
- [7] K. Greisen, *Phys. Rev. Lett.* **16**, 748 (1966); G. T. Zatsepin and V. A. Kuzmin, *JETP Lett.* **4**, 78 (1966) [*Pisma Zh. Eksp. Teor. Fiz.* **4**, 114 (1966)]; V. S. Berezhinsky and S. I. Grigor'eva, *Astron. Astrophys.* **199**, 1 (1988).
- [8] For a review see M. Kachelrieß, *Comptes Rendus Physique* **5**, 441 (2004) [arXiv:hep-ph/0406174].
- [9] F. A. Aharonian, P. S. Coppi and H. J. Völk, *Astrophys. J.* **423**, L5 (1994) [arXiv:astro-ph/9312045].
- [10] A. Neronov and D. V. Semikoz, *JETP Lett.* **85**, 473 (2007) [arXiv:astro-ph/0604607].
- [11] K. Dolag, M. Kachelrieß, S. Ostapchenko and R. Tomàs, *Astrophys. J.* **703**, 1078 (2009) [arXiv:0903.2842 [astro-ph.HE]].
- [12] A. Elyiv, A. Neronov and D. V. Semikoz, *Phys. Rev. D* **80**, 023010 (2009) [arXiv:0903.3649 [astro-ph.CO]].
- [13] R. Plaga, 1995, *Nature*, **374**, 430; K. Murase *et al.*, *Astrophys. J.* **686**, L67 (2008).
- [14] P. d'Avezac, G. Dubus and B. Giebels, *Astron. Astrophys.* **469**, 857 (2007) [arXiv:0704.3910 [astro-ph]]; A. Neronov and I. Vovk, *Science* **328**, 73 (2010) [arXiv:1006.3504 [astro-ph.HE]]; F. Tavecchio *et al.*, *Mon. Not. Roy. Astron. Soc.* **406**, L70 (2010).
- [15] For information on MPI see e.g. "Message Passing Interface Forum. MPI: A Message Passing Interface Standard, June 1995" on <http://www.mpi-forum.org>.
- [16] F. Aharonian *et al.* [H.E.S.S. Collaboration], *Astron. Astrophys.* **475**, L9 (2007) [arXiv:0709.4584 [astro-ph]].
- [17] A. A. Abdo *et al.* [Fermi LAT Collaboration], *Astrophys. J.* **707**, 707 (2009) [arXiv:0910.4881 [astro-ph.HE]].

- [18] V. S. Beresinsky and G. T. Zatsepin, Phys. Lett. B **28**, 423 (1969); Sov. J. Nucl. Phys. **11**, 111 (1970).
- [19] V. Berezhinsky, A. Gazizov, M. Kachelrieß and S. Ostapchenko, Phys. Lett. B **695**, 13 (2011) [arXiv:1003.1496 [astro-ph.HE]].
- [20] A. Elyiv, A. Neronov and D. V. Semikoz, Phys. Rev. D **80**, 023010 (2009) [arXiv:0903.3649 [astro-ph.CO]].
- [21] A. Neronov *et al.*, Astrophys. J. **719**, L130 (2010) [arXiv:1002.4981 [astro-ph.HE]].
- [22] M. Kachelrieß, S. Ostapchenko and R. Tomàs, New J. Phys. **11**, 065017 (2009) [arXiv:0805.2608 [astro-ph]].
- [23] V.N. Baier, V.M. Katkov and V.M. Strakhovenko, “Electromagnetic processes at high energies in oriented single crystals”, World Scientific (1998).
- [24] W. H. Press, S. A. Teukolsky, W. T. Vetterling, B. P. Flannery, Numerical Recipes in Fortran 90, (Cambridge University Press 1996)